Early Events in Protein Aggregation: Molecular Flexibility and Hydrophobicity/Charge Interaction in Amyloid Peptides as Studied by Molecular Dynamics Simulation.

ARTICLE *in* PROTEINS STRUCTURE FUNCTION AND BIOINFORMATICS · JANUARY 2005

Impact Factor: 2.63

Early Events in Protein Aggregation: Molecular Flexibility and Hydrophobicity/Charge Interaction in Amyloid Peptides as Studied by Molecular Dynamics Simulations

Mariacristina Valerio,[1] Alfredo Colosimo,[2] Filippo Conti,[1] Alessandro Giuliani,[3] Alessandro Grottesi,[4] Cesare Manetti,[1] and Joseph P. Zbilut[5]*

[1]*Department of Chemistry, University of Rome "La Sapienza," Rome, Italy*
[2]*Department of Human Physiology and Pharmacology, University of Rome "La Sapienza," Rome, Italy*
[3]*Environment and Health Department, Istituto Superiore di Sanità, Rome, Italy*
[4]*Department of Biochemistry, University of Oxford, Oxford, United Kingdom*
[5]*Department of Molecular Biophysics and Physiology, Rush Medical College, Chicago, Ilinois*

ABSTRACT **In a previous article (Zbilut et al., Biophys J 2003;85:3544–3557), we demonstrated how an aggregation versus folding choice could be approached considering hydrophobicity distribution and charge. In this work, our aim is highlighting the mutual interaction of charge and hydrophobicity distribution in the aggregation process. Use was made of two different peptides, both derived from a transmembrane protein (amyloid precursor protein; APP), namely, Aβ(1-28) and Aβ(1-40). Aβ(1-28) has a much lower aggregation propensity than Aβ(1-40). The results obtained by means of molecular dynamics simulations show that, when submitted to the most "aggregation-prone" environment, corresponding to the isoelectric point and consequently to zero net charge, both peptides acquire their maximum flexibility, but Aβ(1-40) has a definitely higher conformational mobility than Aβ(1-28). The absence of a hydrophobic "tail," which is the most mobile part of the molecule in Aβ(1-40), is the element lacking in Aβ(1-28) for obtaining a "fully aggregating" phenotype. Our results suggest that conformational flexibility, determined by both hydrophobicity and charge effect, is the main mechanistic determinant of aggregation propensity. Proteins 2005;58:110–118.** © 2004 Wiley-Liss, Inc.

Key words: aggregation versus folding; conformational changes; α to β transition; amyloid fibrils; conformational flexibility

INTRODUCTION

Protein aggregation versus folding remains as a persistent problem in molecular biology. Over the past 10 years, studies of protein aggregation have been stimulated by the realization that protein misfolding, with the consequent formation of polymer insoluble aggregates, is involved in degenerative pathologies, of which Alzheimer's, Huntingon's, and prion diseases are striking examples.[1] Moreover, it has been given renewed emphasis with the demonstration that, in principle, any protein is subject to aggregation given appropriate conditions. Any modification of environmental conditions, such as pH, concentration, temperature, ionic strength, metal ions, and so forth, could drive any protein in solution to the formation of multimeric aggregates and eventual precipitation.[2] The molecular basis of the conversion of normally soluble proteins into polymeric insoluble aggregates is still unclear. At the moment, it is commonly accepted that the aggregation pathway occurs via a conformational change that leads the protein to adopt a partially structured conformation in its soluble state. The nature of the intermediate state preceding aggregation has been subject of much investigation. A number of intermediate conformations, ranging from partially unfolded or folded to molten globule or native-like state, have been observed. A common observation is the link between the self-aggregation process and the presence of β-sheet structures: It has been hypothesized that intermediate conformations contain β-sheets and/or they have some increased propensity to adopt a β-sheet structure.[3] Furthermore, the molecules are thought to aggregate through the association between their exposed hydrophobic surfaces.[2,4–6] Although hydrophobicity remains a key factor in this process, as we have discussed in a previous paper,[7] another aspect, namely, protein charge, appears to be an important covariant.[8–10]

In this work, we focus on evaluating pH-dependent conformational changes of the very early dynamical regimen relative to the aggregation process (i.e., the formation of intermediate monomeric conformations), aiming to provide new insights relative to the effect of hydrophobicity and charge distribution on aggregation propensity. To this end, molecular dynamics (MD) simulations provide an opportunity to explore the nature of the early steps of protein aggregation at an atomic level with nanosecond

Grant sponsor: Joint Division of Mathematical Sciences/National Institute of General Medical Sciences initiative to support mathematical biology, from the National Science Foundation and National Institutes of Health; Grant number: NSF DMS 0240230 (J. P. Zbilut, Principal Investigator).

*Correspondence to: Joseph P. Zbilut, Department of Molecular Biophysics and Physiology, Rush Medical College, 1635 W. Congress, Chicago, IL 60612. E-mail: joseph_p_zbilut@rush.edu

Received 26 April 2004; Accepted 18 July 2004

Published online 3 November 2004 in Wiley InterScience (www.interscience.wiley.com). DOI: 10.1002/prot.20306

TABLE I. Composition and Definitions of the Simulated Systems

Peptide	pH	Ionization state of residues	N_0 counterions	Definitions
Aβ(1–40)	2–4	Asp^0, Glu^0, His^+	−6	AB40L
Aβ(1–40)	5–6	Asp^-, Glu^-, His^+	—	AB40M
Aβ(1–40)	7	Asp^-, Glu^-, His^0	+3	AB40N
Aβ(1–28)	2–4	Asp^0, Glu^0, His^+	−6	AB28L
Aβ(1–28)	5–6	Asp^-, Glu^-, His^+	—	AB28M
Aβ(1–28)	7	Asp^-, Glu^-, His^0	+3	AB28N

resolution. In this respect, the choice of an appropriate model that would allow us to focus on the determining variables was important. The significant aspects of the model included a protein with varying hydrophobicity along the chain and the ability to modulate the charged states of the protein by changing pH. A clear choice was the peptides, collectively referred to as "amyloid β-peptide" (Aβ), which are manageably short for MD simulations and at the same time have a large associated experimental literature. Aβ, a 39–43 amino acid residue peptide, is generated from proteolytic processing of the larger transmembrane protein APP, as an ensemble of variant polypeptides manifesting heterogeneity at both chain ends, as well as in nonterminal sequence positions.[11] However, the predominant species with high aggregation propensity are the Aβ(1-40) and Aβ(1-42) peptides.[12,13] Aβ is known to be a soluble protein in healthy individuals but has a high propensity to form β-sheet-enriched aggregates in nerve cells of Alzheimer's disease patients. Through NMR, circular dichroism (CD), and Fourier transform infrared (FTIR) studies, the Aβ peptide has shown a conformational polymorphism; that is, it adopts different secondary structure in different environments (pH, temperature, concentration, presence of metal ions such as Cu^{2+} and Zn^{2+}, and incubation time).[11,14]

For the purpose of our work, we have chosen as model systems the isoforms Aβ(1-28) and Aβ(1-40), which both contain the same ionizable residues but differ in the hydrophobicity profile; the hydrophobic tail (Ile32–Val40) is present only in the full-length fragment. Moreover, experimentally, these 2 peptides have shown a different propensity for aggregation: Aβ(1-28) does not form fibrils and is not plaque-competent in dilute aqueous solutions at every pH tested,[15] while Aβ(1-40) is able to form fibrils over a pH range 5–6 and is plaque-competent in the pH range 5–9, in water.[15–17] Our data, based on the analysis of multiple nanosecond timescale simulations at low (2–4), medium (5–6, near to isoelectric point), and neutral pH, confirm the hypothesis of the major role of hydrophobicity with respect to charge in affecting aggregation propensity.[10] The dynamical counterpart of aggregation propensity was demonstrated to be the relative flexibility of the peptides. The interaction between hydrophobicity distribution and charge mediated by differences in molecular flexibility was also proposed by our group.[7] In this work, we focus on the dynamical subtleties of the process by means of new simulations. Besides confirming the previous results, we demonstrate that the increase in flexibility goes hand in hand with the loss of interaction between the hydrophobic tail and the peptide core, with the tail acting as a "sticky end" for linking other molecules. This behavior is also in line with observations on different aggregating systems.[6]

MATERIAL AND METHODS

Multiple nanosecond timescale simulations of the amyloid β-peptides Aβ(1-40) and Aβ(1-28) were carried out at low (pH range 2–4), medium (pH range 5–6), and neutral pH in explicit solvent water molecules at different initial velocities. Starting atomic coordinates of Aβ(1-28) and Aβ(1-40) were obtained from the Protein Data Bank (PDB), entry code 1AMB,[18] and 1BA4 (8th model),[19] respectively. The different pH states were created by changing the protonation state of the ionizable residues according to their pKa. The site of protonation of all histidines was based on the analysis performed by the program WHATCHECK.[20] To neutralize the systems, salt ions were added. We refer to our previous article[7] for the details of the simulation protocol, summarized below. The simulations were performed in the number, volume, temperature (NVT) ensemble using the GROMACS software packages and the GROMOS96 force field.[21] The SHAKE algorithm[22] was used to constrain bond lengths, with a timestep of 2 fs. Long-range interactions were calculated using the particle mesh Ewald (PME) method.[23] The total length of each simulation was 17 ns long at 300 K. Individual trajectories are defined as follows: Aβ(1-40) simulations at low, medium, and neutral pH are referred to as AB40L, AB40M, and AB40N, respectively; Aβ(1-28) simulations at low, medium, and neutral pH are referred to as AB28L, AB28M, and AB28N, respectively (Table I). To compare different simulations, the structures were classified by the Jarvis–Patrick method with projections into a root-mean-square deviation (RMSD) space.[24] The obtained structures were clustered by means of the Jarvis–Patrick algorithm as applied to their RMSD values. This method allocates 2 structures into the same cluster if they are reciprocal "first neighbors" and share at least 3 common "neighbors." The criterion for considering 2 structures as "first neighbors" is simply being among the first 10 structures with the most similar RMSD. Each simulation is sampled every 10 ps and lasts 17,000 ps, with the results expressed in terms of the subsequent "visits" of the trajectory to the clusters. Only the clusters visited once by the trajectories are discussed with respect to their structural features. This choice derives from Li and Daggett[25,26] and is based on the fact that only those clusters represent

"intermediate states." Secondary structures were assigned by means of the DSSP program.[27]

Quantitative characterization of the dynamical properties of each system was performed using a principal component analysis (PCA) of the covariance matrix of the positional fluctuations of Cα atoms, as previously described.[28–30] This matrix was built from the equilibrated portion of the trajectories (i.e., beyond the first nanosecond), and its diagonalization afforded the principal directions of the large-amplitude concerted motions (principal eigenvectors) that characterize the essential subspace of each protein's internal dynamics. Each element of this matrix is a quantitative measure of the average concerted fluctuation of the *i*th atom with respect to the *j*th atom.

All simulations for each individual systems were qualitatively comparable. Therefore, for simplicity, we show the results obtained from 1 simulation only for each system.

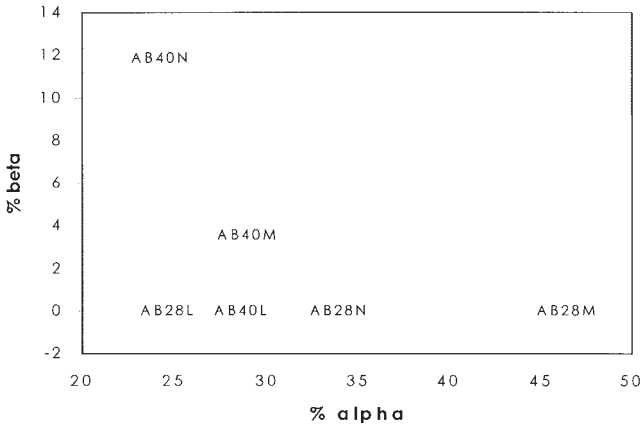

Fig. 1. Percentage of α-helix and β-sheet structure per simulation averaged over the entire trajectory: Aβ(1-28), DAEFRHDSGY EVHHQKLVFF AEDVGSNK; Aβ(1-40), DAEFRHDSGY EVHHQKLVFF AEDVGSNKGA IIGLMVGGVV.

RESULTS AND DISCUSSION

Simulation Conditions

CD and NMR studies have shown that Aβ(1-28) in an aqueous solution containing organic solvents is soluble and adopts predominantly α-helical structure in the pH range 1–4. Within the pH range 4–7, the β-sheet structure is favored and the degree of aggregation is concentration-dependent.[18,31–33] In water, Aβ(1-28) does not form aggregates and instead adopts a random coil structure at low pH. As the pH approaches 5.6 (isoelectric point), above a concentration of 300 μM, the solubility of the peptide decreases, exhibiting flocculant precipitation.[15,31] On the contrary, the Aβ(1-40) monomer exists in α-helical structure in an aqueous solution of organic solvents at any tested pH.[19,34,35] In aqueous buffers, or in water, the monomeric peptide tends to convert to a more extended structure,[36] leading to the transformation of β-sheet-rich aggregates into fibrils within minutes at pH 5–6 (near the isoelectric point) or within days at pH 7–7.5 at high concentration of the peptide or under physiological concentration of NaCl.[15–17] According to these results, Aβ(1-40) shows a much greater aggregation propensity than Aβ(1-28), and the isoelectric pH favors the formation of β-sheet/aggregates. To provide a modelistic insight into the early steps of the aggregation process, the Aβ(1-40) peptide was simulated with explicit water molecules at pH 5–6, starting with a conformation where residues Gly15–Val36 form an α-helix with a kink at residues Gly25–Asn27 (55% α-helical content for the whole peptide). The charge or side-chain ionization effects on the aggregation propensity were evaluated by performing simulations of Aβ(1-40) also at low (1–4) and neutral pH.

We simulated the smaller fragment Aβ(1-28) under identical conditions to evaluate the hydrophobic effect, since it contains mostly hydrophilic amino acids. This allows for the simultaneous evaluation of the influence of charge and hydrophobicity on the aggregation process.

Comparison of Aβ(1-28) and Aβ(1-40) Simulations at Different pH

A general view of the different MD simulations in terms of secondary structure may be provided by a DSSP analysis of secondary structure for the intermediates of each system. Figure 1 reports the percentage of α-helix and β-sheet occurrence per simulation averaged over the entire trajectory. Tables II and III instead report the secondary structure profile of the different trajectories at different timesteps. Figure 1 shows how conditions with varying aggregation propensity display more or less the same fraction of α-helix and β-sheet conformations. The percent occurrence, averaged over the complete simulations of AB40M and AB40N, as a function of residue number, revealed that the β-sheet conformation has about the same extent, involving the region spanning from residues Asp23 to Gly37 (Fig. 2). This indicates that even if aggregated systems are actually richer in β-sheets with respect to monomers, the formation of β-sheets is unable to discriminate the dynamical behavior concerning different aggregation propensity conditions, at least in the early steps of the aggregation process.

Since the relative content of β-sheets per se cannot discriminate between the 2 experimentally proven differential aggregation propensities of Aβ(1-40) at pH 5–6 and pH 7, it seems necessary to consider the dynamical details of conformational transitions; consequently, we focus on Aβ(1-40), which experimental evidence indicates is much more aggregation prone as compared to Aβ(1-28). To get a better appreciation of the relative conformational stability of the trajectories, we analyze the MD simulation under the aspect of tertiary structure clusters. A MD simulation remaining in the same (or few) cluster, may explore only a limited portion of the conformational space, pointing to a stable situation and, consequently, to a low number of conformational transitions. However, an MD simulation characterized by an elevated number of clusters and rich dynamics between different configurations (clusters) points to a more flexible system. It is fair to conclude that conformational flexibility depends on both the number of conformational clusters typical of each trajectory and the number of flippings between different clusters (conformational transitions). Thus, the general profile of conformational flexibility of different systems is defined by 3

TABLE II. Average Secondary Structure Content of Aβ(1-28) Calculated Within Each Cluster l_x, m_x, and n_x, of AB28L, AB28M, and AB28N Trajectories, Respectively, According to DSSP Criteria

		Secondary Structure						
Clusters	Time Period (ps)	Coil	β-sheet	Bend	Turn	α-helix	π-helix	3_{10}-helix
	Starting structure[a]	22.5	—	12.5	10.0	55.0	—	—
l_1	(8660–9090)	16.6 (2.1)[b]	—	4.0 (2.1)	2.1 (3.2)	32.9 (5.9)	44.3 (7.1)	—
l_2	(9100–11,100)	16.0 (3.5)	—	5.9 (3.1)	3.9 (4.7)	26.4 (7.5)	47.6 (8.7)	0.1 (1.1)
l_3	(15,090–15,410)	12.4 (2.7)	—	7.3 (2.4)	13.0 (9.3)	22.2 (9.8)	45.1 (15.5)	—
l_4	(15,420–16,480)	19.3 (2.9)	—	7.0 (3.1)	4.6 (4.9)	18.6 (12.1)	50.2 (13.4)	0.2 (1.5)
l_5	(16,490–16,610)	19.9 (1.8)	—	5.6 (1.8)	8.2 (6.3)	14.3 (10.8)	52.0 (5.7)	—
l_6	(16,620–16,900)	21.0 (3.0)	—	6.3 (3.1)	5.1 (4.5)	17.8 (7.2)	49.4 (8.8)	0.4 (2.1)
l_7	(16,910–17,000)	17.9 (2.4)	—	5.8 (4.1)	3.3 (4.1)	21.1 (5.3)	51.9 (5.3)	—
m_1	(16,010–16,430)	11.1 (0.3)	—	—	15.4 (8.2)	59.6 (11.1)	12.1 (11.1)	1.1 (4.3)
m_2	(16,440–16,820)	14.3 (0.0)	—	1.4 (2.5)	17.9 (8.9)	50.7 (11.1)	15.7 (13.2)	—
m_3	(16,830–17,000)	14.3 (0.0)	—	0.3 (0.7)	15.0 (8.6)	49.3 (11.1)	20.7 (16.8)	0.7 (2.5)
n_1	(2280–5420)	18.8 (3.2)	1.8 (2.9)	3.7 (4.3)	19.2 (5.5)	54.8 (4.5)	0.9 (4.1)	0.6 (2.4)
n_2	(5430–6880)	15.2 (3.8)	2.5 (3.4)	9.4 (4.9)	21.3 (6.8)	51.5 (5.6)	0.1 (1.0)	—
n_3	(6890–8290)	16.4 (2.9)	—	7.8 (4.6)	12.3 (8.3)	51.8 (8.5)	11.3 (16.3)	0.3 (1.6)
n_4	(8300–8410)	17.9 (0.0)	—	—	12.4 (5.5)	35.9 (4.8)	33.9 (7.8)	—
n_5	(8420–9990)	17.7 (0.7)	—	8.6 (3.3)	9.3 (6.0)	7.6 (9.7)	56.2 (10.6)	0.5 (2.1)
n_6	(10,000–17,000)	20.8 (1.5)	—	0.5 (1.5)	6.6 (6.2)	15.9 (12.5)	56.0 (14.4)	0.2 (1.5)

[a]The corresponding reference values in the NMR structure (referred as starting structure[18]) are also reported.
[b]Standard deviations are given in parentheses.
Only the clusters visited once by the trajectories are reported.

TABLE III. Average Secondary Structure Content of Aβ(1–40) Calculated Within Each Cluster L_x, M_x, and N_x, of AB40L, AB40M, and AB40N Trajectories, Respectively, According to DSSP Criteria

		Secondary Structure						
Clusters	Time Period (ps)	Coil	β-sheet	Bend	Turn	α-helix	π-helix	3_{10}-helix
	Starting structure[a]	22.5		12.5	10.0	55.0		
L_1	(0–1670)	30.5 (4.5)[b]	—	16.5 (6.0)	8.3 (6.8)	44.3 (11.0)	—	—
L_2	(1680–1890)	32.3 (4.0)	—	29.0 (4.5)	9.3 (3.3)	29.3 (1.5)	—	—
L_3	(6070–7360)	35.3 (4.0)	—	20.8 (4.0)	7.5 (5.5)	25.8 (1.5)	7.8 (6.3)	3.0
L_4	(7370–11,470)	29.3 (3.8)	—	22.3 (5.3)	14.0 (6.3)	27.3 (1.5)	1.5 (4.3)	5.3
L_5	(11,480–12,230)	35.0 (2.5)	—	19.8 (4.0)	10.8 (4.5)	26.8 (1.3)	4.0 (4.3)	4.0
L_6	(12,240–15,770)	35.0 (4.5)	—	20.0 (3.5)	9.8 (5.5)	26.5 (2.0)	5.8 (6.3)	—
L_7	(15,780–17,000)	31.8 (5.5)	—	25.8 (4.8)	9.0 (7.0)	27.8 (2.3)	7.5 (6.3)	—
M_1	(0–310)	25.3 (2.0)	—	14.0 (3.0)	2.3 (3.0)	58.5 (2.7)	—	—
M_2	(320–2770)	17.5 (5.0)	—	19.5 (5.5)	8.3 (6.8)	48.3 (5.8)	6.5 (7.3)	—
M_3	(13,080–13,600)	24.3 (2.5)	19.8 (5.0)	10.3 (3.0)	27.8 (4.5)	17.8 (3.0)	—	—
M_4	(14,020–15,620)	23.0 (4.3)	18.0 (4.5)	15.5 (5.0)	27.0 (5.5)	16.5 (3.8)	—	—
M_5	(15,630–17,000)	16.5 (2.5)	19.0 (8.8)	14.0 (7.5)	34.0 (5.3)	16.3 (4.5)	—	—
N_1	(0–4620)	28.6 (3.3)	7.5 (3.3)	9.6 (4.2)	11.3 (7.0)	38.1 (12.3)	4.1 (8.2)	—
N_2	(4630–8430)	28.9 (3.2)	15.7 (3.8)	8.3 (3.2)	20.6 (6.2)	19.6 (6.2)	7.0 (10.1)	—
N_3	(13,500–15,670)	22.6 (4.2)	15.5 (4.3)	13.5 (3.7)	21.5 (6.4)	13.9 (5.6)	13.4 (11.1)	—
N_4	(15,680–16,730)	26.1 (2.1)	16.6 (3.3)	9.7 (2.8)	22.4 (6.0)	16.7 (4.2)	8.7 (8.2)	—
N_5	(16,740–17,000)	26.3 (2.2)	16.9 (2.5)	9.6 (2.9)	31.3 (4.7)	14.9 (4.0)	1.0 (4.3)	—

[a]The corresponding reference values in the NMR structure (referred as starting structure[19]) are also reported.
[b]Standard deviations are given in parentheses.
Only the clusters visited once by the trajectories are reported.

variables: number of clusters visited; number of conformational transitions; and maximal number of transitions corresponding to the number of transitions between the 2 specific clusters showing the higher number of mutual interconversions. As indicated in Table IV, the situation with the highest propensity for fibrillation (AB40M) shows the richest conformational dynamics: The state space of the trajectory can be subdivided into 52 clusters among which the system oscillates 193 times during the 17,000 ps of the simulation. On the contrary, the most "prohibitive"

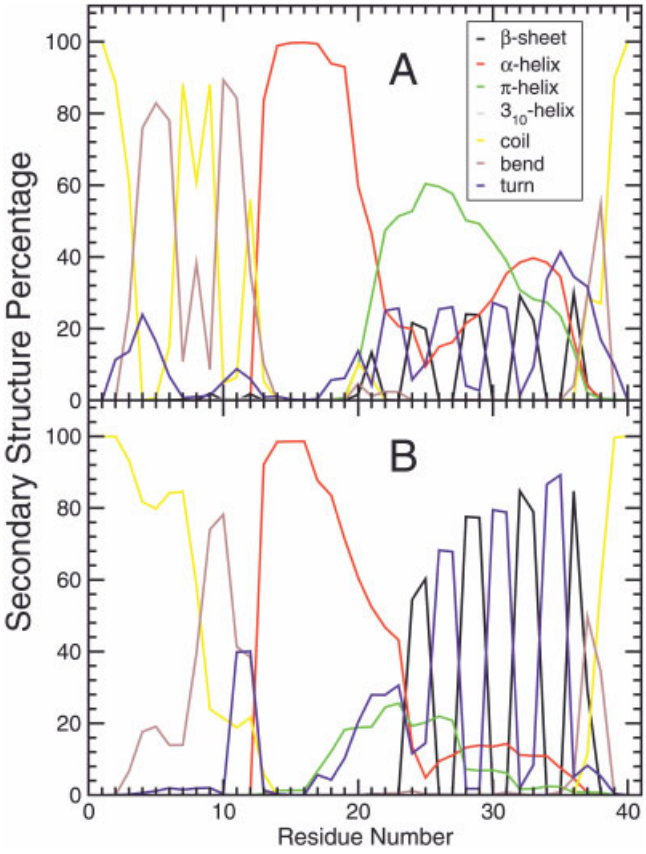

Fig. 2. Percentage of secondary structure per residue averaged over the complete simulation of AB40M (**A**) and AB40N (**B**).

TABLE IV. Indexes of Conformational Flexibility for Each Trajectory

Simulated Systems	N_0 clusters	N_0 transition	N_0 transition max between two specific clusters
AB40L	17	34	3
AB40M	52	193	8
AB40N	8	13	2
AB28L	21	65	3
AB28M	30	94	5
AB28N	8	10	2

environment for fibrillation (AB40N) has only 8 clusters, which the trajectory visits with 13 oscillations.

Indicators of Conformational Flexibility

Conformational flexibility is thus described by 3 different indexes: (1) number of different conformational clusters visited during the simulation; (2) number of transitions between clusters; and (3) maximal number of transitions between 2 specific clusters. The 3 indexes are strongly correlated (Pearson's r near to unity), which allows for a straightforward discrimination of the most flexible simulation. At first sight, it is evident that AB40M is by far the most flexible system and that AB28M is the most flexible preparation of the 3 Aβ(1-28) systems examined. It is worth noting that the large difference in flexibility between Aβ(1-40) and Aβ(1-28) is only evident at

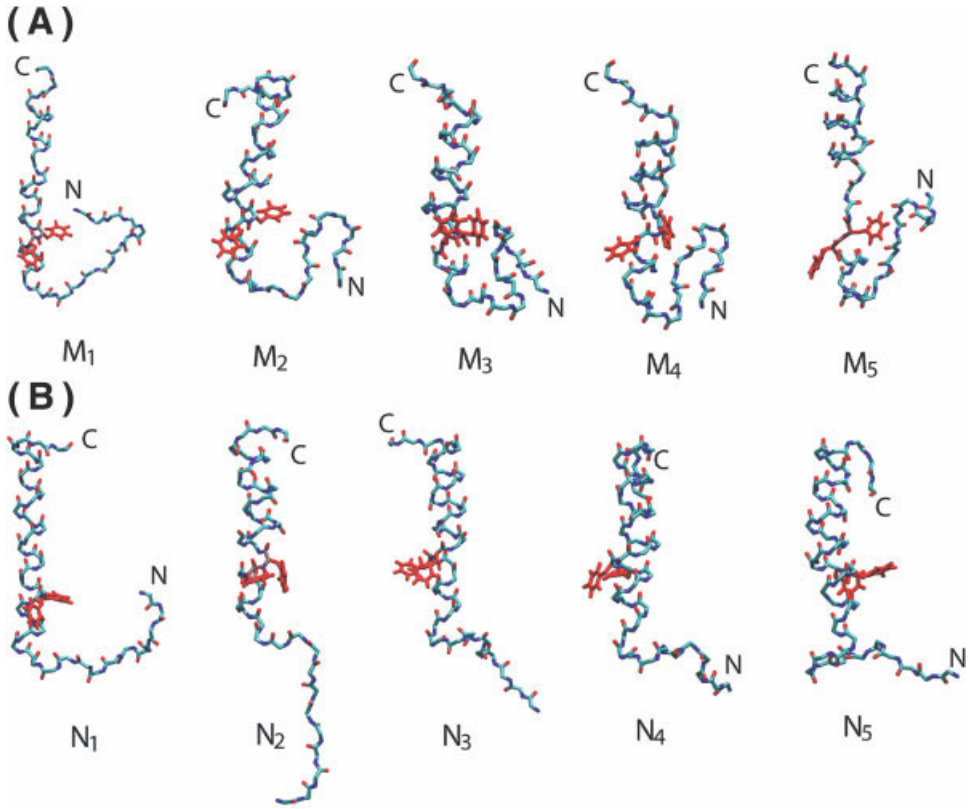

Fig. 7. Stick representation of the 6 representative structures for each cluster of AB40M (**A**) and AB40N (**B**) visited once by the trajectories. The N and C labels indicate the N- and C-termini, respectively. Phe-20 and Phe-21 side-chains are represented in red.

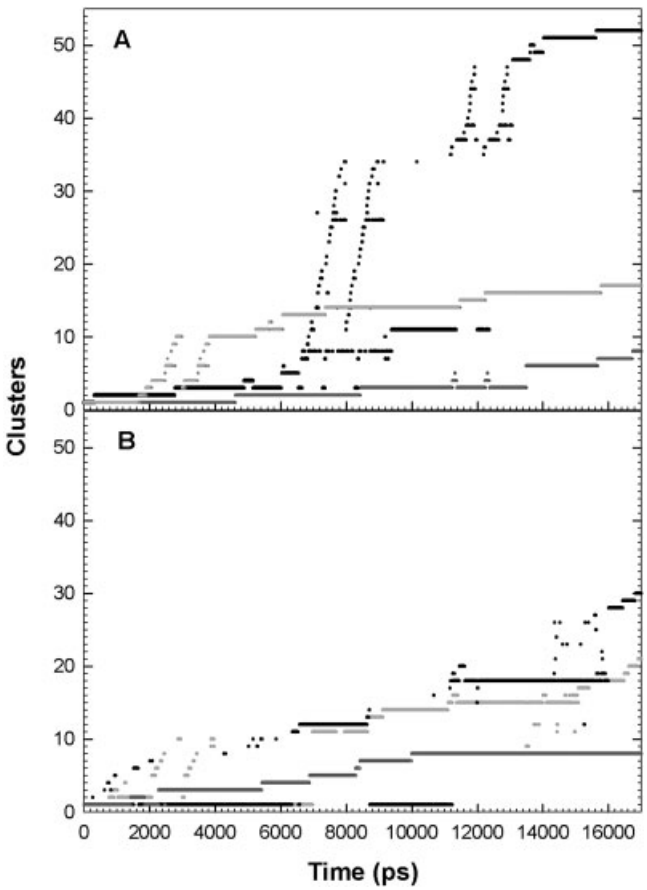

Fig. 3. Clusters as a function of time for Aβ(1-40) (**A**) and Aβ(1-28) (**B**). Color code is as follows: gray (pH range 2–4); black (pH range 5–6); dark gray (pH 7).

medium (aggregation prone) pH, thus confirming the proposed relationships between conformational flexibility and aggregation propensity. Figure 3(A and B) allows for the appreciation of these differences from a graphical point of view. It is worth noting the alternation of very rapid conformational changes characterized by very steep portions of the curve and relatively "flat" periods in which the peptides explore a relatively narrow conformational domain. The major presence of a π-helix in AB40M is confined in the steep portion of the dynamics (6600–17,000 ps), thus confirming its role of a structurally transient intermediate. The lack of the hydrophobic tail in Aβ(1-28) seems to drastically reduce the conformational flexibility of the molecule with respect to Aβ(1-40). While it may be trivial to observe that a larger system like Aβ(1-40) has a greater conformational domain than a smaller one, it is worth noting that the hydrophobic tail is the portion of the molecule endowed with the greater flexibility.

To summarize the above dynamical picture, we submitted to a PCA the fluctuations of the Cα atoms positions at different pH's, and Figure 4 shows the atomic mean displacement along the first eigenvector for pH 5–6 and pH 7 in the case of Aβ(1-40). The figure indicates that the region beyond residue 20 of Aβ(1-40) is more flexible at pH 5–6 than at pH 7. An analogous behavior is present also along eigenvectors 2 and 3 (data not shown). However, since the first principal component spans about 40% of the overall protein fluctuations, results highlighted by eigenvector 1 are indicative of the different degree of flexibility in the highly hydrophobic C-terminal region of AB40 at different pHs.

The flexibility of the protein backbone was analyzed over the whole simulation time by calculating the standard deviations (SDs) averaged from backbone torsion angles, ϕ and ψ, as shown in Figure 5 for the 3 systems. All the systems show higher backbone flexibility in the N-terminal and C-terminal regions, with SD values between 50° and 110° (data not shown), while a reduction in flexibility is observed in a small patch from His13 and Val18, which is in α-helical conformation along all the simulations. The greater difference occurs in the hydrophobic core region, where, in AB40M, the ψ torsion angles of Phe19 and Phe20 reach values of 68° and 70°, respectively. These data are in qualitative accordance with the experimental data by the Gazit group, who demonstrated the crucial role of stacking interactions between aromatic residues for the aggregation process. The authors hypothesize that the interaction between the 2 Phe residues influences both the energetic content and the directionality of the aggregation phenomenon.[37–40]

Molecular Flexibility and Ionizable Residues

Why is the flexibility favored at medium pH? To mimic the different experimental conditions, we changed only the protonation states of titratable residues. The solvent was not altered. To explain the role of medium pH for increased flexibility, the interactions involving the Glu, Asp, and His residues were evaluated in the AB40M and AB40N simulations. These analyses revealed that hydrogen bonds, Arg5–Glu22 and Arg5–Asp23 at both pH's (5–6 and 7), and His6–Glu22 only at medium pH, were involved in salt bridges. These interactions concern residues known to play important roles in Aβ fibril production and stability. The E22Q Dutch mutant,[41–47] the E22G Arctic mutant,[48] and the E22K Italian mutant[49,50] are known to be associated with Alzheimer's disease. Mutations were made in the Aβ peptide, where Asp23 was replaced by neutral residues, and the results indicated that this residue was particularly important in the formation of amyloid β-sheet structures. Wurth et al.[51] observed that 3 variants containing replacement of His6 showed a solubility enhancement in Aβ(1-42). The electrostatic interaction between His6 and Glu22 generates different correlated motions in the AB40M system with respect to AB40N, as depicted in Figure 6(B), where the presence of quite correlated motions, and hence of a decreased flexibility, in the C terminal region at pH 7 is represented by the strong lines parallel to the main diagonal. Such lines link the hydrophobic core (residues 17–21) to the tail, and are much less evident at pH 5–6 [Fig. 6(A)], indicating, in the latter case, a greater conformational richness of the structure.

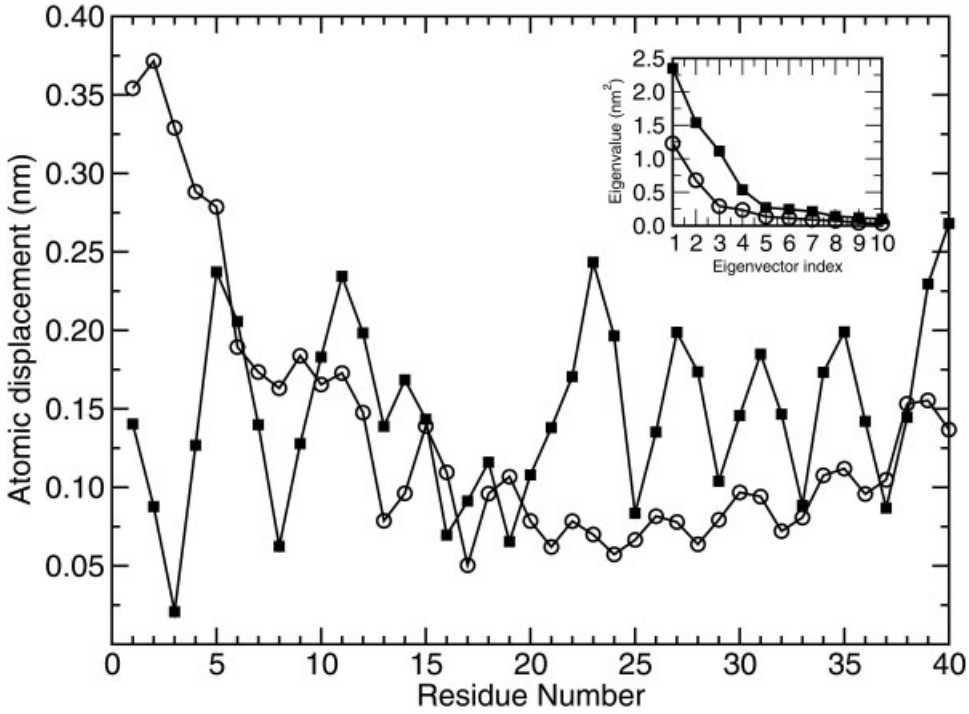

Fig. 4. Mean atomic displacement along eigenvector 1 of the Cα atoms of the Aβ(1-40) at pH 5 to 6 (■) and 7 (○). Insets: Eigenvalue spectra of the essential subspace (first 10 eigenvectors) at pH 5–6 (■) and pH 7 (○).

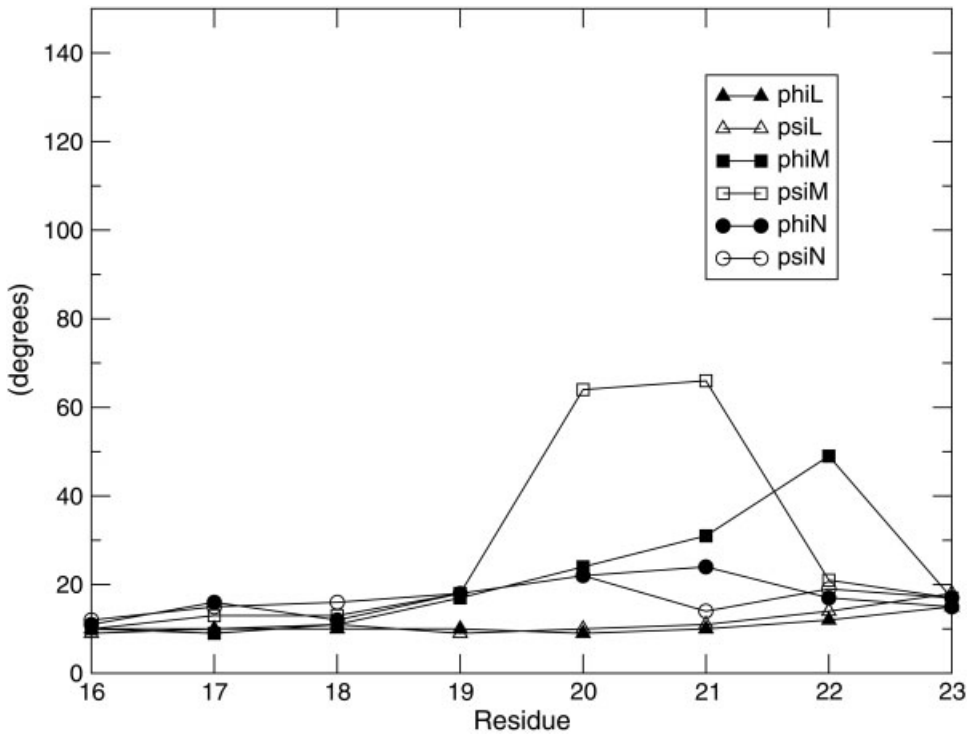

Fig. 5. Standard deviations (SDs) of the backbone torsion angles, ϕ (filled symbols) and ψ (open symbols) for AB40L (triangle), AB40M (square), and AB40N (circle).

CONCLUSIONS

The most immediate finding of our work in comparing MD simulations of Aβ(1-28) and Aβ(1-40) is that molecular flexibility is the main determinant of aggregation propensity: While both systems attain their maximum flexibility at the isoelectric point, Aβ(1-40), the most aggregation-

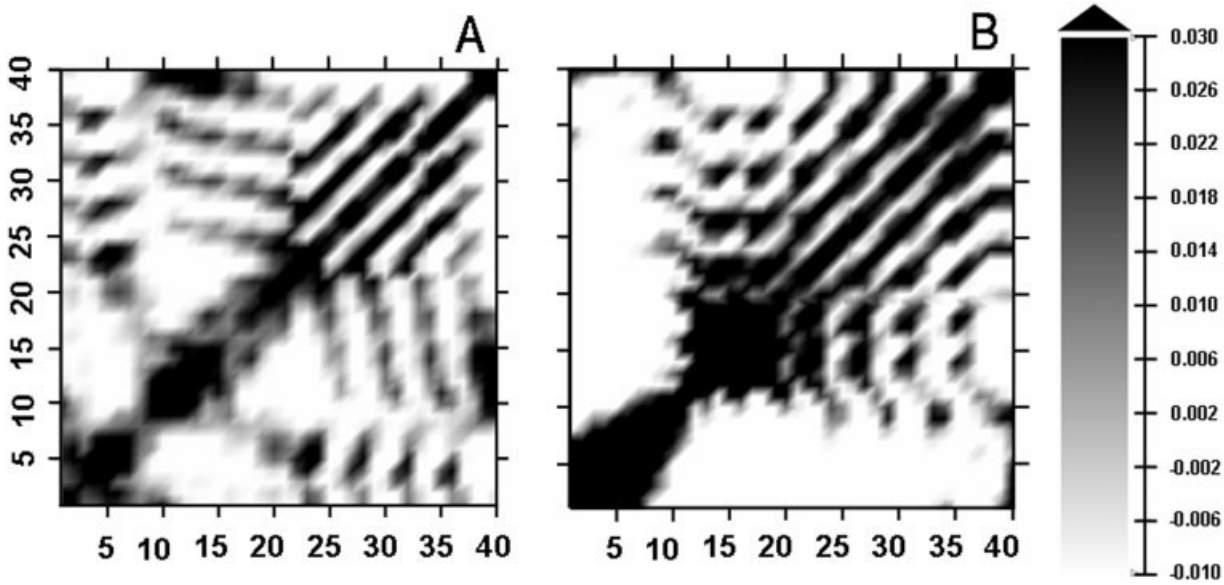

Fig. 6. Atomic covariance maps of the coordinates fluctuations of Cα: AB40M (**A**); AB40N (**B**). The color code on the right indicates the magnitude of the covariance of each elements.

prone species, undergoes a much higher number of conformational transitions than the other system.

In particular, we note that neutral (AB40N) and medium (AB40M) pH conditions produce an almost identical proportion of β-sheets and α-helices, despite the fact that AB40M is much more aggregation-prone than AB40N. Thus, even if the formation of β-sheets is typical of aggregating systems, it does not appear as the main determinant of the aggregation/folding choice. This observation is reinforced by the consistency between the secondary structure composition we observed at neutral pH with the secondary structure content of Aβ(1-40) observed by Walsh et al.[52]

The most relevant structural difference we could observe between AB40M and AB40N is linked to the behavior of the hydrophobic tail (residues 32–40). In AB40N, such a tail appears to be interacting with the hydrophobic core (residues 17–21). On the contrary, in the most aggregation-prone condition (AB40M), a sort of bend appears between His6 and Glu22, stabilized by electrostatic interaction. This bend eliminates the interaction between the hydrophobic core and the tail that is now free to move and to interact with other molecules [Fig. 7(A and B)]. The proposed mechanism implies a strict interplay between hydrophobicity and charge relative to the aggregation phenotype. It is also relevant that mutations of residue Glu22, forming the electrostatic interaction with residue His6, are known to provoke an altered fibrillogenesis propensity.[41–47,50,53]

Our results point to molecular flexibility, influenced by the interplay between hydrophobicity distribution and charge, as the main determinant of protein aggregation. This is in full agreement with the results of the Chiti group,[10,54] who found that hydrophobic interactions have a greater influence as compared to net charge in the aggregation process; although clearly, the net charge effect is a kind of "boundary condition." Even if we are well aware that the use of the monomeric form of the peptides forces us to limit our considerations to the very first steps of the aggregation process, and that the subsequent organization of these oligomers into long and structured fibrils remains out of the reach of our simulations, a comparison between our dynamic approach and the static one by Chiti et al.[54] is also possible. They estimated the relative importance of hydrophobicity and charge in protein aggregation by using a function determined from experimental studies of acylphosphatase. This function depends on 3 physicochemical factors: change in hydrophobicity, overall charge, and propensity to convert from α-helix to β-sheet. In our dynamic approach, all these factors find a direct counterpart in what we observe in terms of hydrophobic effect, charge, and conformational flexibility, respectively, on the nanoseconds timescale.

REFERENCES

1. Dobson CM. Protein folding and disease: a view from the first Horizon Symposium. Nat Rev Drug Discov 2003;2:154–160.
2. Chiti F, Taddei N, Baroni F, Capanni C, Stefani M, Ramponi G, Dobson CM. Kinetic partitioning of protein folding and aggregation. Nat Struct Biol 2002;9:137–143.
3. Rochet JC, Lansbury PT Jr. Amyloid fibrillogenesis: themes and variations. Curr Opin Struct Biol 2000;10:60–68.
4. Lumry R, Eyring H. Conformation changes of proteins. J Phys Chem 1954;58:110–120.
5. Chiti F, Webster P, Taddei N, Clark A, Stefani M, Ramponi G, Dobson CM. Designing conditions for in vitro formation of amyloid protofilaments and fibrils. Proc Natl Acad Sci USA 1999;96:3590–3594.
6. Burke MG, Woscholsky R, Yaliraki SN. Differential hydrophobicity drives self-assembly in Huntington's disease. Proc Natl Acad Sci USA 2003;100:13928–13933.
7. Zbilut JP, Colosimo A, Conti F, Colafranceschi M, Manetti C, Valerio M, Webber CL, Giuliani A. Protein aggregation/folding: the role of deterministic singularities of sequence hydrophobicity as determined by nonlinear signal analysis of acylphosphatase and Aβ(1-40). Biophys J 2003;85:3544–3557.
8. Chiti F, Calamai M, Taddei N, Stefani M, Ramponi G. Studies of the aggregation of mutant proteins in vitro provide insights into

the genetics of amyloid diseases. Proc Natl Acad Sci USA 2002;99: 16419–16426.
9. Schmittschmitt JP Scholtz JM. The role of protein stability, solubility, and net charge in amyloid fibril formation. Protein Sci 2003;12:2374–2378.
10. Calamai M, Taddei N, Stefani M, Ramponi G, Chiti F. Relative influence of hydrophobicity and net charge in the aggregation of two homologous proteins. Biochemistry 2003;42:15078–15083.
11. Serpell LC. Alzheimer's amyloid fibrils: structure and assembly. Biochim Biophys Acta 2000;1502:16–20.
12. Roher AE, Lowenson JD, Clarke S, Woods AS, Cotter RJ, Gowing E, Ball MJ. β-Amyloid-(1-42) is a major component of cerebrovascular amyloid deposits: implications for the pathology of Alzheimer disease. Proc Natl Acad Sci USA 1993;90:10836–10840.
13. Selkoe DJ. Alzheimer's disease: genes, proteins, and therapy. Physiol Rev 2001;81:741–766.
14. Lynn DG, Meredith SC. Review: model peptides and the physicochemical approach to β-amyloids. J Struct Biol 2000;130:153–173.
15. Lee J, Stimson E, Ghilardi J, Mantyh Y, Lu A, Felix A, Llanos W, Behbin A, Cummings M, Van Criekinge M, Timms W, Maggio J. ^{1}H NMR of Aβ amyloid peptide congeners in water solution: conformational changes with plaque competence. Biochemistry 1995;34:5191–5200.
16. Harper JD, Wong SS, Lieber CM, Lansbury PT. Assembly of Aβ amyloid protofibrils: an in vitro model for a possible early event in Alzheimer's disease. Biochemistry 1999;38:8972–8980.
17. Inouye H, Kirschner DA. 2000. Aβ fibrillogenesis: kinetic parameters for fibril formation from Congo Red binding. J Struct Biol 2000;130:123–129.
18. Talafous J, Marcinowsky KJ, Klopman J, Zagorsky MG. Solution structure of residues (1-28) of the amyloid beta-peptide. Biochemestry 1994;33:7788–7796.
19. Coles M, Bicknell W, Watson AA, Fairlie DP, Craik DJ. Solution structure of amyloid beta-peptide(1-40) in a water–micelle enviroment: Is the membrane-spanning domain where we think it is? Biochemistry 1998;37:11064–11077.
20. Hooft RWW, Vriend G, Sander C, Abola E. Errors in protein structures. Nature 1996;381(6580):272.
21. van der Spoel D, Berendesen HJC, van Buuren AR, Apol MEF, Meulenhoff PJ, Sijbers ALTM. Gromacs user manual. Groningen, The Netherlands: Niienborgh; 1995.
22. Ryckaert JP, Ciccotti G, Berendsen HJC. Numerical integration of the Cartesian equations of motion of a system with costraints: molecular dynamics of n-alkanes. J Comp Phys 1997;23:327–341.
23. Darden T, York D, Pedersen L. Particle mesh Ewald: an N*log(N) method for computing Ewald sums. J Chem Phys 1993;98:10089–1092.
24. Jarvis RA, Patrick EA. Clustering using a similarity measure based on shared near neighbors. IEEE Trans Comput 1973;C22: 1025–1034.
25. Li A, Daggett V. Characterization of the transition state of protein unfolding by use of molecular dynamics: chymotrypsin inhibitor 2. Proc Natl Acad Sci USA 1994;91:10430–10434.
26. Li A, Daggett V. Identification and characterization og the unfolding transitino state of chymotrypsin inhibitor 2 by molecular dynamics simulations. J Mol Biol 1996;257:412–429.
27. Kabsch W, Sanders C. Dictionary of protein secondary structure: pattern recognition of hydrogen-bonded and geometrical features. Biopolymers 1983;22:2577–2637.
28. Garcia AE. Large-amplitude nonlinear motions in proteins. Phys Rev Lett 1992;68:2696–2699.
29. Amadei A, Linssen ABM, Berendsen HJC. Essential dynamics of proteins. Proteins 1993;7:412–425.
30. Wong CF, Zheng C, Shen J, McCammon A, Wolynes PG. Cytochrome c: a molecular proving ground for computer simulations. J Phys Chem 1993;97:3100–3110.
31. Barrow CJ, Zagorsky MG. Solution structure of β-peptide and its constituent fragments relation to amyloid deposition. Science 1991;253:179–182.
32. Barrow CJ, Yasuda A, Kenny PTM, Zagorsky MG. Solution conformations and aggregational properties of synthetic amyloid β-peptide of Alzheimer's disease. J Mol Biol 1992;225:1075–1093.
33. Zagorsky M, Barrow C. NMR studies of amyloid β-peptide: Proton assignments, secondary structure and mechanism of an α-helix-β-sheet conversion for a homologous, 28 residue, N-terminal fragment. Biochemistry 1992;31:5621–5631.
34. Soto C, Castano E, Frangione B, Inestrosa N. The α-helical to β-sheet transition in the amino-terminal fragment of the amyloid β-peptide modulates amyloid formation. J Biol Chem 1995;270: 3063–3067.
35. Sticht H, Bayer P, Willbold D, Dames S, Hilbich C, Beyreuther RF, Rosch P. Structure of amyloid A4(1-40)-peptide of Alzheimer's disease. Eur J Biochem 1995;233:293–298.
36. Zagorsky MG, Shao H, Ma K, Yang J, Li H, Zeng H, Zhang Y, Papilla M. Aβ(1-40) and Aβ(1-42) adopt remarkably stable monomeric and extended structures in water solution at neutral pH. Neurobiol Aging 2000;21:S10–S11.
37. Gazit E. Mechanistic studies of the process of amyloid fibrils formation by the use of peptide fragments and analogues: implication for the design of fibrillization inhibitors. Curr Med Chem 2002;9:1725–1735.
38. Azriel R, Gazit E. Analysis of the minimal amyloid-forming fragment of the islet amyloid polypeptide: an experimental support for the key role of the phenylalanine residue in amyloid formation. J Biol Chem 2001;276:34156–34161.
39. Mazor Y, Coilead S, Benhar I, Gazit E. Identification and characterization of a novel molecular-recognition and self-assembly domain within the islet amyloid polypeptide. J Mol Biol 2002;322: 1013–1024.
40. Reches M, Porat Y, Gazit E. Amyloid fibril formation by pentapeptide and tetrapeptide fragments of human calcitonin. J Mol Biol 2002;277:35475–35480.
41. Levy E, Carman MD, Fernandez-Madrid IJ, Power MD, Lieberburg I, van Duinen SG, Bots GT, Luyendijk W, Frangione B. Mutation of the Alzheimer's disease amyloid gene in hereditary cerebral hemorrhage, Duch-type. Science 1990;248:1124–1126.
42. Fraser PE, Nguyen JT, Inouye H, Surewicz WK, Selkoe DJ, Podlisny MB, Kirschner DA. Fibril formation by primate, rodent, and Dutch-hemorrhagic analogues of Alzheimer amyloid β-protein. Biochemistry 1992;31:10716–10723.
43. Davis J, Van Nostrand WE. Enhanced pathologic properties of Duch-type mutant amyloid β-protein. Proc Natl Acad Sci USA 1996;93:2996–3000.
44. Watson DJ, Selkoe DJ, Teplow DB. Effects of the amyloid precursor protein glu^{693}→gln "duch" mutation on the production and stability of amyloid β-protein. Biochem J 1999;340:703–709.
45. Esler WP, Felix AM, Stimson ER, Lachenmann MJ, Ghilardi JR, Lu Y, Vinters HV, Mantyh PW, Lee JP, Maggio JE. Activation barriers to structural transition determine deposition rates of Alzheimer's disease. J Struct Biol 2000;130:174–183.
46. Melchor JP, McVoy L, Van Nostrand WE. Charge alterations of e22 enhance the pathogenic properties of the amyloid β-protein. J Neurochem 2000;74:2209–2212.
47. Sian AK, Frears ER, El-Agnaf OA, Patel BP, Manca MF, Siligardi G, Hussein R, Austen BM. Oligomerization of β-amyloid of the Alzheimer's and the Dutch-cerebral-haemorrage. Biochem J 2000; 349:299–308.
48. Nilsberth C, Westlind-Danielsson A, Eckman CB, Condron MM, Axelman K, Forsell C, Stenh C, Luthman J, Teplow DB, Younkin SG, Naslund J, Lannfelt L. The "Artic" APP mutation (E693G) causes Alzheimer's disease by enhanced Aβ protofibril formation. Nat Neurosci 2001;4:887–893.
49. Bugiani O, Padovani A, Mangoni M, Andora G, Sgarzi M, Savoiardo M. An Italian type of HCHWA. Neurobiol Aging 1998;19: S238.
50. Miraville L, Tokuda T, Charlie R, Giaccone G, Bugiani O, Bavaglini F, Frangine B, Ghiso J. Substitution at codon 22 of Alzheimer's Aβ induce diverse conformational changes and apoptotic effects in human cerebral endothelial cells. J Biol Chem 2000;275: 27110–27116.
51. Wurth C, Guimard NK, Hecht MK. Mutations that reduce aggregation on the Alzheimer's Aβ42 peptide: an unbiased search for the sequence determinants of Aβ amyloidogenesis. J Mol Biol 2002;319:1279–1290.
52. Walsh MD, Hartley DM, Kusumoto Y, Fezoui Y, Condron MM, Lomakin A, Benedek GB, Selkoe DJ, Teplow DB. Amyloid β-protein fibrillogenesis. J Biol Chem 1999;274:25945–25952.
53. Wisniewsky T, Ghiso J, Frangione B. Peptides homologous to the amyloid protein of Alzheimer's disease containing a glutamine for glutamic acid substitution have accelerated amyloid fibril formation. Biochem Biophys Res Commun 1991;179:1247–1254.
54. Chiti F, Stefani M, Taddei N, Ramponi G, Dobson CM. Razionalization of the effects of mutations on peptide and protein aggregation rates. Nature 2003;424:805–808.